Materials Science & Engineering A 798 (2020) 140119

Contents lists available at ScienceDirect

Materials Science & Engineering A

journal homepage: http://www.elsevier.com/locate/msea

Thermal stabilization of additively manufactured superalloys through defect engineering and precipitate interactions

Michael Munther [a], Russell A. Rowe [a], Montu Sharma [b], Lloyd Hackel [b,**], Keivan Davami [a,*]

[a] Department of Mechanical Engineering, The University of Alabama, Tuscaloosa, AL, USA
[b] Metal Improvement Company, Surface Technologies, Curtiss Wright, Livermore, CA, USA

ARTICLE INFO

Keywords:
Thermal stabilization
Laser peening
Microstructure engineering
Inconel

ABSTRACT

Laser peening (LP) is a mechanical surface modification technique capable of enhancing a treated material's resistance to surface-related failures through the introduction of deep, high-magnitude compressive residual stresses. Conventional LP enables material improvement in systems operating in ambient or low temperature ($<0.5T_m$ where T_m is the melting temperature) conditions. At high temperature ($>0.5T_m$), LP-induced property enhancements and microstructural modifications encounter thermal degradation through dislocation annihilation, stress relaxation, and grain coarsening. Motivated by the need to retain critical material enhancements, a novel, modified LP technique was introduced and employed in this work, coined laser peening plus thermal microstructure engineering (LP + TME). This approach incorporates cyclic LP events with the inclusion of intermittent, 600 °C ($0.55T_m$) heat treatment steps in order to impart highly thermally stable microstructural modifications in additively manufactured (AM) Inconel 718. Microstructural and mechanical property evolution was evaluated through instrumented indentation and transmission electron microscopy (TEM). Surface-level compressive residual stresses were discovered to increase by as much as 84% from 167.13 MPa to over 300 MPa following LP + TME and a 350-h, 600 °C exposure. Surface and near-surface microhardness of samples subjected to LP + TME was observed to increase by 33% (to 630 HV) compared to untreated, as-built specimens even after exposure to 600 °C. Hardened zones were characterized by the presence of highly dense dislocation networks and precipitated strengthening phases. Both property enhancement and thermal stability were determined to be the result of various mechanisms at work, stemming from the synergistic combination of cyclic strain and thermal input. These include the facilitated nucleation of γ'' and δ phases which aid in stabilizing LP-induced microstructures and provide material enhancements at high temperatures; precipitate-dislocation interactions including Orowan bypassing, Friedel cutting; and dislocation pinning effects. The results from this work are of significant interest as they are in contrast with what is typically expected at temperatures exceeding $0.5T_m$ meaning the technique outlined herein could offer a viable solution to overcoming obstacles preventing the widespread use of LP in critical, high temperature applications.

1. Introduction

Laser peening is a post-processing technique used for the optimization of service lives of critical components by generating high density of dislocations, inducing compressive residual stresses in the surface and sub-surface (as deep as 12 mm) of treated components. These compressive residual stresses are usually accompanied by an increase in microhardness, enhancing the material's resistance to surface-related failures such as creep [1], fatigue [2], foreign object damage [3,4], and stress corrosion cracking [5,6]. While the LP process enhances the life span and durability of the material, the induced compressive residual stresses of LP relax at high temperatures ($>0.5T_m$, where T_m is the melting temperature), limiting the applicability of the technique. At temperatures above $0.5T_m$, significant thermal relaxation takes place in Inconel 718 when temperatures are high enough to cause annihilation and reorganization of the crystalline defects induced by the peening process, and to reduce the material's yield stress [7].

The relaxation behavior of residual stresses from LP is primarily

* Corresponding author.
** Corresponding author.
E-mail addresses: Lloyd.Hackel@cwst.com (L. Hackel), kdavami@eng.ua.edu (K. Davami).

https://doi.org/10.1016/j.msea.2020.140119
Received 6 May 2020; Received in revised form 11 August 2020; Accepted 16 August 2020
Available online 19 August 2020

caused by three main mechanisms; mechanical, thermal and thermo-mechanical [8]. Thermo-mechanical relaxation mechanisms are relatively complex processes and are attributed to both thermal and mechanical effects. Thermal relaxation mechanisms result from the rearrangement of meta-stable crystalline defects such as dislocations, and relaxation effects relate to the plasticity of materials. In mechanical relaxation, the superposition of applied stress and residual stress reach the yield strength of the material and that might even cause plastic deformation. The thermal relaxation of residual stresses at elevated temperatures results from the annihilation and reorganization of LP-induced crystalline defects, creep controlled dislocation rearrangement, and the softening of the material at higher temperatures [9]. These phenomena lead to the relaxation of residual stresses in laser peened specimens when exposed to high temperatures, limiting the application of conventional laser shock peening techniques [7,10–12]. At sufficiently high temperatures, solid state diffusion also leads to additional difficulties in obtaining thermal stability in laser peened materials. This mechanism influences not only dislocation density but also the microstructural barriers impeding dislocation motion. Thus high temperature exposure enables dislocation recovery through climb and recombination at a significant rate, and precipitate and grain coarsening or dissolution, rendering all of the available microstructural barriers inoperative [13].

Previous studies have identified the complications associated with the implementation of LP in high temperature applications wherein the effects of thermal and cyclic loading on the stability of LP-induced microstructural modifications were analyzed [14–18]. Most notably, *Kattoura* et al. scrutinized the thermal stability of LP-induced microstructural changes in traditionally manufactured nickel-based superalloys [19]. Residual stress relaxation experiments of multi-layered laser peened Inconel 718/718 Plus found a 65% retention of near surface compressive residual stresses after 120 h at 650 °C [16,20]. It was discovered that between 25% and 60% of initial values of LP-induced residual stresses were preserved after one million fatigue loading cycles at 650 °C.

Compressive residual stress retention and stability at high temperatures after cyclic loading in LPed specimens have been attributed to three mechanisms: (1) low amounts of cold work, (2) the formation of high density dislocations and strong slip bands, and (3) pinning effect of precipitates at elevated temperatures [7,21,22]. With clear and promising evidence of residual stress and microstructure stability, an effective technique to apply LP that retains residual stress has yet to be developed. Attempts, however, have been made to maximize the stability of LP-induced microstructural changes and their associated fatigue and surface strength enhancement. *Cheng* et al. introduced and performed warm laser shock peening (WLP), or LP performed at elevated temperatures (160 °C) on various materials, and found significant overall increases in microstructure stability, fatigue life, and surface strength when compared to conventional, room temperature treatment in Al 6061 [23], Al 7075 [24], Ti–6Al–4V [25], AISI 4140 [26], and 1042 stainless steels [27]. These increases are thought to be mainly contributed to the pinning effect of LP-induced dislocation and subgrain formation [28]. Additionally, thermal engineered LP (TE-LP), which is the combination of a single WLP and subsequent one-step heat treatment was found to increase the pinning effect of precipitates [29,30].

It is therefore the objective of the work outlined herein to develop a systematic approach to understanding the mechanistic origins of both material enhancement and thermal stability in additively manufactured Inconel 718 following LP + TME treatment. The effectiveness of the LP + TME process was evaluated from a material property and microstructural standpoint. Transmission electron microscopy (TEM) and chemical analyses through energy dispersive x-ray spectroscopy (EDX) were undertaken to investigate the microstructural mechanisms driving residual stress and microhardness variations following surface treatments.

2. Experimental methods

2.1. Sample fabrication and preparation

The additively manufactured specimens treated and analyzed in this work were fabricated by means of direct metal laser sintering (DMLS, *MBFZ Toolcraft GmbH, Germany*), using a standard 200 W Inconel 718 parameter set. A layer height of 30 μm was employed throughout the building process. Specimen dimensions were 120 mm in length, 11 mm in width, and 21 mm in height. From the larger, as-built bulk samples, 4 identical cubic specimens measuring 5 mm × 5 mm × 5 mm were cut via electrical discharge machining (EDM). Samples were then ground using progressively finer grits, then polished using a colloidal silica suspension.

2.2. Laser peening and heat treatment

Selected samples analyzed in this work underwent LP or a combination of both heat treatment and LP. Laser peening was carried out using a 1054 nm flash pumped Nd glass laser delivering 16 J per pulse on target, with a beam irradiance of 8 GW/cm^2. A square, 3 mm^2 spot and 18 ns (full width half height) pulse duration with approximately 0.7 ns risetime was employed for all treatments. Selected LP samples were also subjected to intermittent thermal treatments occurring between successive LP events. Intervening heat treatment was performed in an open-air furnace operated at 600 °C (0.55T_m) for a duration of 8 h, and the AM-4LP-3HT-E sample was subjected to a final thermal exposure at 600 °C for 350 h. Temperature was chosen as commercial turbine engine blades can reach temperatures up to 600 °C for 2 min during takeoff, and assuming a blade lifespan of 10,500 takeoffs, a 350-h exposure was selected [31]. The various combinations of LP and heat treatment employed to treat the samples studied in this work can be seen outlined in Table 1. An as-built, untreated specimen was also included in the experimental undertakings in order to generate an accurate frame of reference.

2.3. Electron microscopy

Transmission electron microscopy (TEM, *FEI Tecnai F-20*) foils were sectioned from the top (treated) surfaces of each specimen through focused ion beam (FIB) milling. Foils were approximately 10 μm in length and 5 μm in width, encapsulating the affected region of the material. TEM imaging was carried out in order to visualize precipitation morphology, dislocation density, and microstructural evolution with and without treatment.

2.4. Vickers microhardness

Vickers microhardness measurements were performed using a Vickers microhardness tester (*Clemex Technologies Inc., Canada*) with the

Table 1
Sample treatment details. 1 × 8 GW/cm2 relates to a single LP shot with an irradiance of 8 GW/cm2; 4 × 8 GW/cm2 relates to four LP shots with identical irradiance. HT refers to the intervening heat treatments at 600 °C for 8 h, and E represents a thermal exposure at 600 °C for 350 h.

Sample Name	Laser Peening	Heat Treatment	Surface Polish
AM	None	None	Grinding, colloidal silica
AM-LP	1 × 8 GW/cm^2, 18 ns pulse	None	Grinding, colloidal silica
AM-4LP-3HT	4 × 8 GW/cm^2, 18 ns pulse	3 × 600 °C, 8 h	Grinding, colloidal silica
AM-4LP-3HT-E	4 × 8 GW/cm^2, 18 ns pulse	3 × 600 °C, 8 h; 1 × 600 °C, 350 h	Grinding, colloidal silica

aim of investigating the penetrative depth of the shockwave and any accompanying microhardness enhancements. A Vickers indenter tip operated at 300 gf (~3 N) was employed in generating a 30 × 20 indent matrix in the topmost section within the treated region, totaling 600 indents for each sample. Resulting Vickers microhardness (HV) results were organized into a matrix format where the data was smoothed, and then contoured to generate a microhardness profile throughout the depth of the material. The total measured region for each sample was 3000 μm × 2000 μm.

2.5. Residual stress

Compressive residual stresses imparted into the various target specimens studied in this work were measured through x-ray diffraction

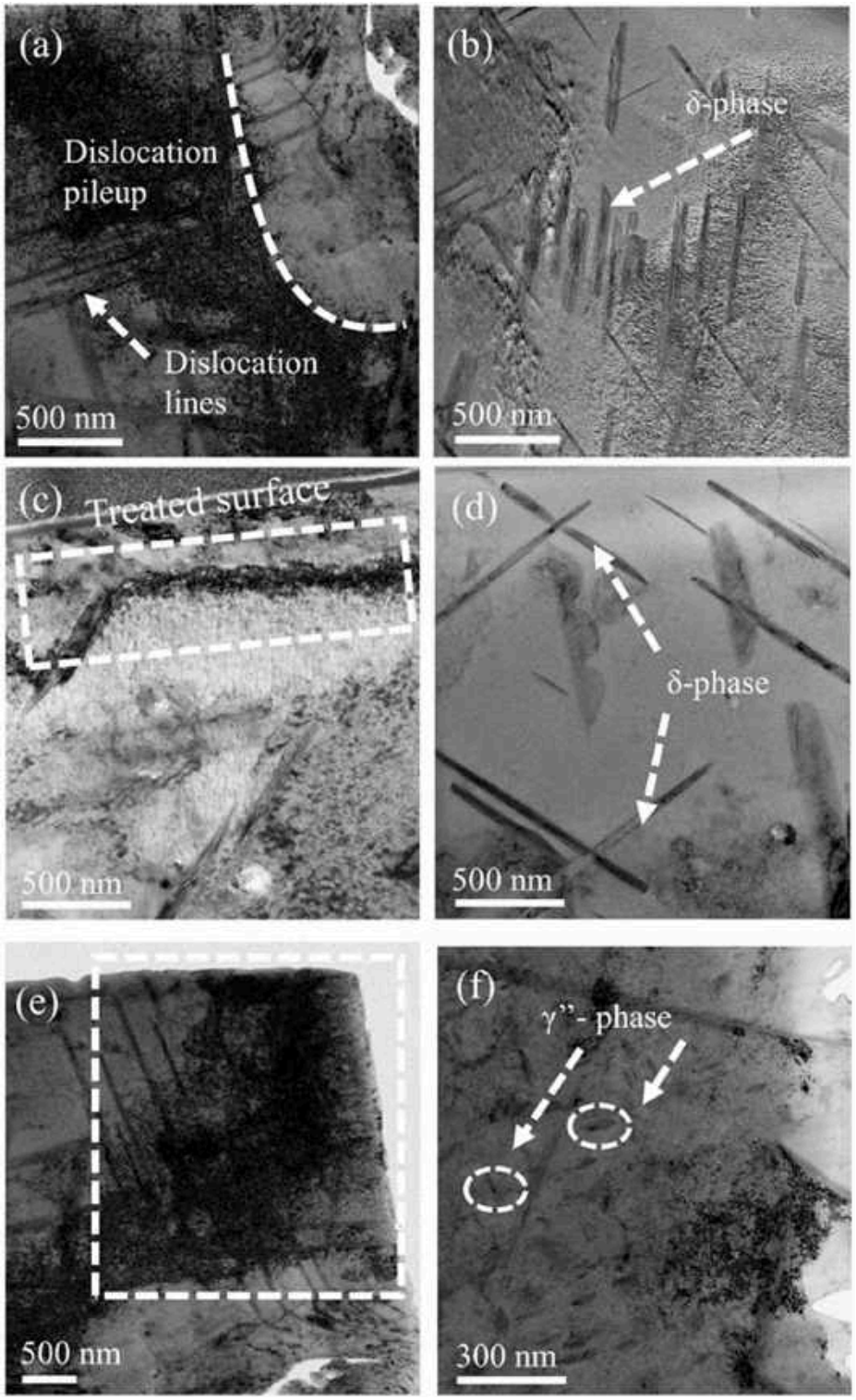

Fig. 1. TEM micrographs of (a) AM sample, highlighting the presence of highly dense dislocations, (b) presence of δ-phase in the AM matrix, (c) presence of highly dense dislocations in the AM-LP sample, (d) additional evidence for intermediate phase formation, (e) large, surface-level dislocation network in the AM-4LP-3HT-E sample, and (f) solid-state coherent precipitates discovered in AM-4LP-3HT-E.

(XRD) with a single axis goniometer using Ω geometry (*Proto iXRD*). The conventional sin 2ψ technique was employed to extract relevant compressive residual stress values. Device alignment and calibration were verified before each measurement using a standard, stress-free 316 L steel powder sample. The measured values in the stress-free specimen were less than ±12 MPa and in the range recommended by manufacturers. The device was equipped with Mn Kα x-ray source (λ = 2.10314 Å), operated with a 1 mm aperture size. Measurements were taken from the surface of each material, both treated and as-built.

3. Results

3.1. Microstructure

TEM micrographs obtained from the top ~5 μm of each of the three Inconel specimens can be seen in Fig. 1. Fig. 1a illustrates the presence of high density, near-surface dislocations in the AM sample. As this sample was characterized in its as-built state without any surface modifications, the origin of these dislocation structures (tangles and lines) is a result of the additive fabrication wherein the repeated melt-solidification induces thermal stresses within the material. During the DMLS process, a high energy laser-focused zone undergoes rapid heating and cooling. This rapid cooling and heating introduces thermal stress variations that cause areas of the additively manufactured layers to expand and contract at different rates, generating a high density of dislocations [32].

TEM investigations unveiled the presence of the orthorhombic, nonequilibrium δ (Ni_3Nb) phase, which is seen to precipitate with a clearly ordered *'chessboard'* distribution, shown in Fig. 1b. This specific phase precipitation results from Nb segregation originating during the DMLS process. Moreover, the unique distribution illustrated in Fig. 1b is regulated by the build direction, where this phenomenon has been observed in previous studies on DMLS Inconel 718 dislocations [32]. Fig. 1c displays a TEM micrograph of the surface and near-surface regions of the AM-LP sample. Here, high density dislocations are observed throughout the material, as seen in the AM sample. However, unlike the AM sample, the AM-LP specimen exhibits isolated dislocation structures reserved to the top ~300 nm of the material. It is clear that this dislocation superstructure is a direct result of the attenuation of the high intensity shockwave throughout the material, severely plastically deforming the surface and immediate sub-surface. In Fig. 1d the precipitation of needle-like δ phases arranged in a chessboard-like orientation was again observed. The TEM micrographs taken of the AM-4LP-3HT-E sample can be seen in Fig. 1e and f. Fig. 1e highlights the extent of the dislocation structure after repeated laser shocks, with this structure extending approximately 2 μm into the depth of the material (highlighted by the white box). Achieving a dislocation structure of this depth results from the repeated laser shock treatment, taking advantage of a larger number of activatable slip planes, driving previous dislocations deeper into the material with each subsequent shock [33]. In Fig. 1f, TEM revealed the presence of solid-state precipitates, namely γ'' (Ni_3Nb), an ordered super-lattice form of the FCC-Al Ni-rich matrix [34,35].

Phase identification was carried out through energy dispersive x-ray spectroscopy (EDX). Element mapping was employed to distinguish the chemistry of detected intermediate phases, namely δ and γ'. Displayed in Fig. 2 are instances of visual detection of γ'' and δ phases and corresponding element maps. While both δ and γ'' are chemically identical per their phase formula (Ni_3Nb), non-insignificant concentrations of Ti and Cr have also been detected in the chemistry of γ'' and δ phases [36,37]. A TEM micrograph of an area situated in the near-surface region of

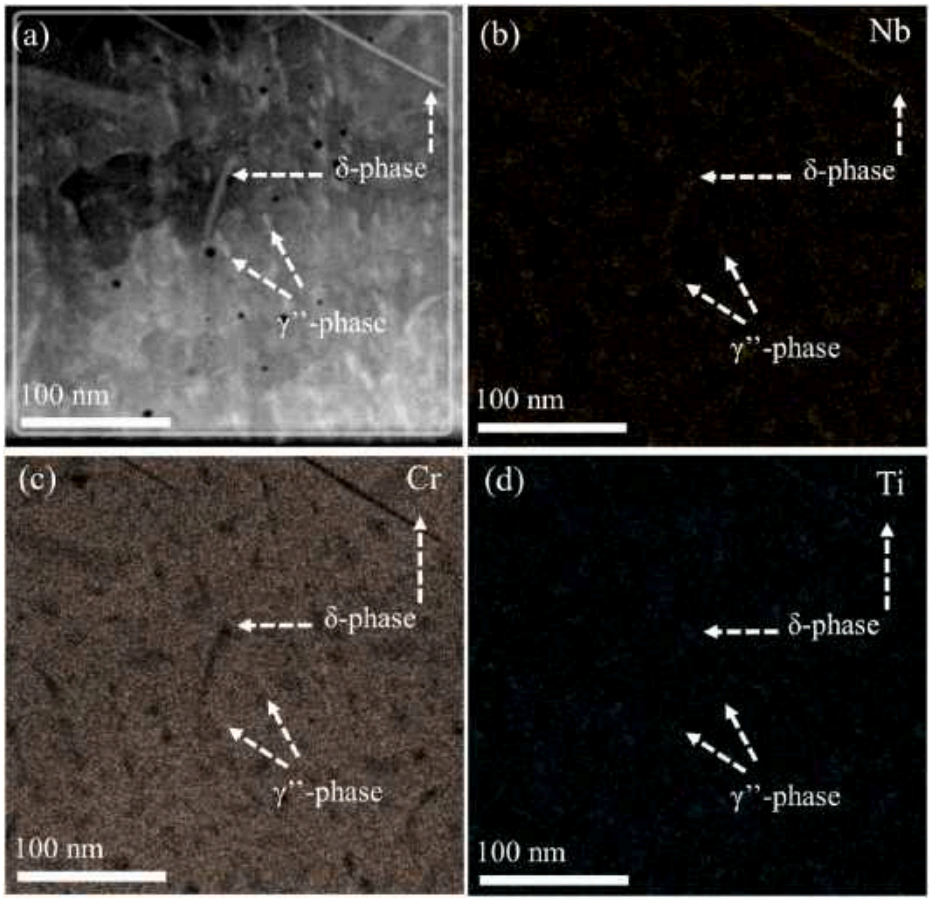

Fig. 2. TEM micrograph showing the presence of precipitated δ and γ'' phases, and respective EDX elemental maps showing (b) Nb; (c) Cr; and (d) Ti content taken from (a).

sample subjected to AM-4LP-3HT-E can be seen in Fig. 2a, highlighting the presence of precipitated γ'' and δ phases. Furthermore, elemental maps displaying Nb, Cr, and Ti concentrations can be seen in Fig. 2b, c, and 2d, respectively. In each, γ'' was observed to precipitate as disk-shaped, or platelet-like morphologies. Alternatively, δ was found to have precipitated as acicular, or needle-like morphologies.

3.2. Residual stress

Residual stress measurements were undertaken to evaluate the fidelity of LP-induced compressive residual stresses before and after heat treatments, and to evaluate the effectiveness of the LP + TME process in not only producing but retaining compressive residual stresses. Surface-level residual stress values can be seen in Fig. 3 for each, AM, AM-LP, and AM-4LP-3HT-E material. A compressive residual stress of −167.13 ± 15.79 MPa was measured from the surface of the untreated, as-built (AM) sample. It is thought the origin of surface-level residual stresses originated during the DMLS build process through intense localized heating, and the repeated melting of previously solidified material [38,39]. Furthermore, *Sochalski-Kolbus* et al. posited that the presence of crystallographic texture which induces microstrain on the system produces variations in measured residual stresses in as-built material as illustrated in Fig. 3 [40]. Additionally, in DMLS Ti-6AL-4V, for example, surface-level compressive residual stresses were located above underlying residual tensile stress fields [41]. An increase in measured residual stresses can be seen for the AM-LP material subjected to a single shot to −194.99 ± 17.065 MPa, an approximate 17% increase over the AM material. These findings are in relative agreement with previous studied highlighting the effects of laser peening in unprotected Inconel 718 [42]. Here, the increase in residual stresses is most likely attributed to the plastic deformation at the surface and propagation and attenuation of the shockwave originating from the irradiated surface. As the shockwaves moves throughout the depth of the material, residual plastic strain generates a compressive residual stress gradient below the target surface [43].

Significant residual stress intensification was measured for the AM-4LP-3HT-E material subjected to LP + TME and a 350-h exposure to 600 °C with stress values reaching −308.505 ± 41.82 MPa, a 58% increase over AM-LP and an 84% increase when compared to the as-built, untreated AM material. In a similar fashion to AM-LP, the repeated introduction of high pressure shock waves generates high magnitude plastic strain accompanied by the formation of compressive residual stresses. It is worth noting that this increase in residual stresses was obtained following a 350-h, 600 °C heat treatment, indicating that this process shows potential in retaining beneficial compressive residual stresses in high temperature environments. In comparison with previous results illustrating the relaxation of LP-induced residual stresses to the findings of the current work, *Telang* et al. [44] reported a decrease in surface-level compressive residual stresses to −100 MPa from −600 MPa following a 24-h, 600 °C thermal exposure (blue diamond marker in Fig. 3). In their work, Inconel 718 was subject to a single shock with an energy density of 9 GW/cm^2, using a 2 mm-diameter beam and with a 50% overlap ratio. This result was presented alongside the findings of the current work in Fig. 3, under the LP-E (laser peen-exposure) heading.

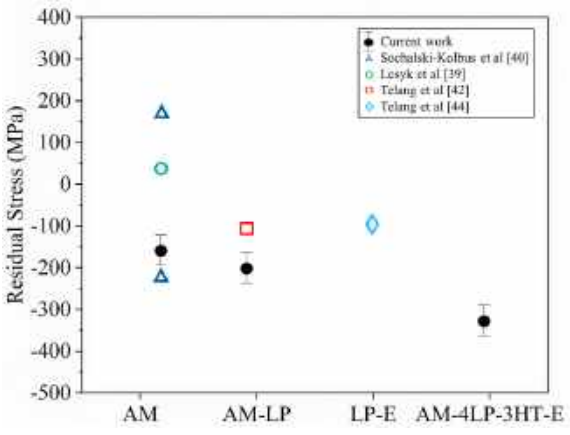

Fig. 3. Surface-level residual stress values of AM, AM-LP, and AM-LP-3HT-E materials studied in this work alongside previous reports on surface-level residual stresses in as-built additively manufactured Inconel 718, Inconel 718 subject to a single LP shot, and laser peened Inconel 718 subject to a 24-h, 600 °C exposure (LP-E).

3.3. Microhardness

Vickers microhardness contour maps of each sample can be seen in Fig. 4 where the *Y-Axis* represents the depth of the measured region, and *X-Axis* represents its width. Fig. 4a displays the measured microhardness distribution for the untreated, AM sample. Here, no clear microhardness trend exists with microhardness values ranging from 450 HV to 515 HV. It should be noted that local microhardness enhancement is thought to be attributed to the apparent random distribution of dislocation networks and intermediate phase formation resulting from the DMLS process. Alternatively, Fig. 4b exhibits the microhardness distribution for the AM-LP sample. In comparison, a perceivable microhardness trend was observed with microhardness decreasing throughout the depth of the material. The most significant microhardness enhancements were reserved to the top ~400 μm, with microhardness values ranging from 520 HV to maximum values exceeding 550 HV, and an average microhardness value of 504 HV. Here, surface-level dislocation networks resulting from shockwave attenuation and the introduction of compressive residual stresses enable the isolated microhardness improvement. As seen in Fig. 3, the increase in residual compressive stresses is thought to be entirely responsible for the measured microhardness enhancement with a 17% increase in compressive residual stresses relating to an approximate 8% increase in average, surface-level microhardness. The microhardness profile of the material subjected to four LP shots and three heat treatments (AM-4LP-3HT) is depicted in Fig. 4c. Striking microhardness variances can be seen here, with the extent of the microhardness increase being localized in the top ~600 nm of the material. The average microhardness of the measured region was observed to be approximately 530 HV, with peak microhardness values exceeding 647 HV, a nearly 5% increase in average microhardness over the AM-LP sample, and an 8% higher average than the untreated, AM sample. A similar microhardness trend was observed in the sample subjected to four LP, three heat treatments, and ending in a final exposure at 600 °C for 350 h (Fig. 4d). Here, there is a clear, isolated microhardness enhancement reserved to the top ~500 nm, with peak values exceeding 630 HV and a measured averaged microhardness of 515 HV. Comparing the highest degree of increases in microhardness which are isolated to the topmost region of the measured area, it is reasonable to conclude that the high-magnitude compressive residual stresses present in the surface of the AM-4LP-3HT-E material (Fig. 3) are driving these microhardness enhancements. Compared to the AM-4LP-3HT sample, this is only a 3% decrease in average hardness after exposure at 600 °C (0.55 T_m) for 350 h, highlighting the effectiveness of the method employed herein at stabilizing the beneficial LP-induced microstructural modifications and induced residual stresses.

4. Discussion

The observed increase in measured microhardness and compressive residual stresses of the LP + TME-treated material, while unexpected, are of significant interest as they offer fundamental insight into thermal stability and material enhancement mechanisms at work following LP + TME. Typically, significant residual stress relaxation as well as surface and near-surface microstructural evolution would be observed at 600 °C

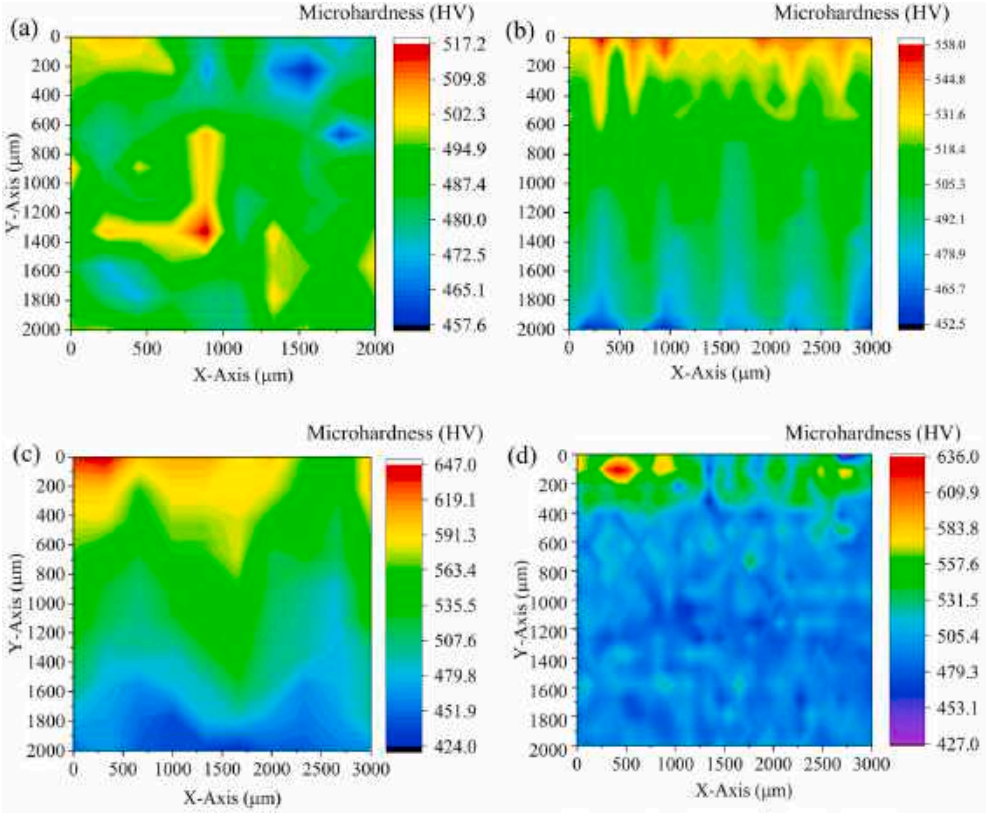

Fig. 4. Microardness contour maps of (a) AM, (b) AM-LP, and (c) AM-4LP-3HT, and (d) AM-4LP-3HT-E specimens. *Y-Axis* represents the depth of the measured region while Y = 0 represents the surface of the specimen that was laser peened; *X-Axis* represents the width of the measured region.

including annihilation, grain coarsening, and the reorganization of meta-stable crystalline defects induced by the LP process [45]. It is therefore suggested that there exists a beneficial, additive effect when employing both LP and intermittent heat treatments, yielding both thermal stability, surface property enhancement, and residual stress retention. This is thought to be attributed to two dominant mechanisms present throughout this process which benefit from both LP and thermal input including: (i) the modification of strengthening phase precipitation kinetics, and (ii) precipitation-dislocation interactions resulting in observed instances of both Orowan and Friedel mechanisms, and pinning effects.

In Inconel 718, the main precipitates that contribute to high temperature strength are the body-centered tetragonal (BCT) coherent γ''-phase and face-centered cubic (FCC) coherent γ′-phase, where γ'' is the main strengthening phase [46–48]. Moreover, the properties of Inconel 718 are mainly governed by the size, volume fraction, and morphology of both γ'' and δ-phases [49–51]. Therefore, the ability to modify the precipitation kinetics of these phases in order to promote early precipitation is crucial, especially for the γ''-phase. Previous studies illustrating the effects of strain on the precipitation kinetics of γ'' and δ-phases in Inconel 718 have found the onset temperature required for precipitation decreases as dislocations resulting from strain input acted as preferential nucleation sites [46,52]. *Mei* et al. [46] investigated the precipitation kinetics of intermediate phases of Inconel 718 and found that with an increased amount of cold rolling, the solvus temperature of γ'' and δ-phases decreased and facilitated precipitation at temperatures outside of the conventional range. In the case of this work, repeated strain input through cyclic LP and intermittent 600 °C heat treatments provide an ideal environment for the early precipitation of γ''. Typically, γ'' precipitation occurs between 600 °C and 900 °C [45], but with the addition of cyclic LP and accompanying plastic deformation, it is surmised that γ'' precipitation occurs below this threshold, leading to an increase in the volume fraction of γ''-phases in the treated surface and near-surface regions at 600 °C. In addition to this, the final thermal exposure for 350 h at 600 °C utilized in the AM-4LP-3HT-E sample is also thought to be contributing to the precipitation of γ''-phases.

Fig. 5 displays TEM micrographs of each sample wherein γ'' content is compared between them. For the AM, and AM-LP samples, Fig. 5a and b, respectively, virtually no γ''-phase content was discovered. It is evident that this is a result of the lack of thermal input, preventing potential phase precipitation. In Fig. 5c, however, a significant increase in γ'' was detected following cyclic LP and thermal loading. In this case where LP precedes thermal treatment (AM-4LP-3HT-E), there are significantly more nucleation sites in the form of dislocation structures, allowing for the early, preferential nucleation of γ'' (Fig. 5c). The presence of the nonequilibrium δ-phase, while small compared to γ'' concentration, is also worth noting as it has been observed to be an effective pinning point for meta-stable crystalline defects and a contributor to controlling excessive grain growth [53]. In the case of the AM-4LP-3HT-E sample, δ-phase precipitation is hypothesized to be the effect of γ''→ δ transformation occurring as a result of γ'' saturation and a reduction of the δ solvus temperature. δ-phase precipitation is usually observed between 750 °C–1020 °C, however the addition of cyclic strain input and the high availability of γ'' enables its early nucleation following γ'' formation [54].

In this work, cyclic strain and thermal input has been hypothesized to enable the early precipitation of critical intermediate phases suspected to be contributing to the appreciable surface microhardness enhancements at $0.55T_m$. This is ultimately a result of dislocation-precipitate interaction wherein meta-stable crystalline defects generated through repeated strain input are stabilized by the preferential nucleation in or around dislocation networks. Here, thermal stability and microhardness enhancement is formulated to be the result of dislocation pinning effects which act to hinder strain- or thermally-driven dislocation movement [35,55]. Fig. 6 exhibits instances of

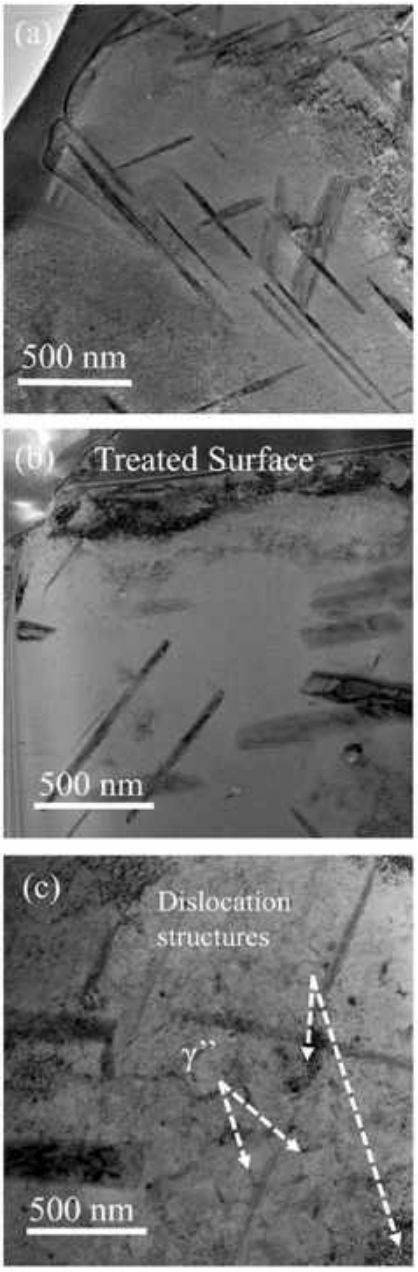

Fig. 5. TEM micrographs illustrating γ'' content in (a) AM, (b) AM-LP, and (c) AM-4LP-3HT-E.

identifiable dislocation pinning in each of the treated samples. Needle-like δ-phases precipitated inside a high density dislocation network in the AM-LP sample is illustrated in Fig. 5a. Here, the preferential nucleation of δ-phase precipitates in these dislocation networks act as an impedance to dislocation migration. Likewise, in Fig. 6b, further evidence of dislocation pinning was observed in the AM-4LP-3HT-E sample subjected to cyclic thermal and strain input. Again, elongated δ-phases are seen interacting with isolated dislocation networks. A clear example of δ-phase pinning effect can be seen in Fig. 6b.

While cases of larger δ-phases effectively hindering mobile dislocations have been visualized, it is suspected that a more dominant stabilizing and strengthening mechanism lies in the interaction between dislocations and finer precipitated particles. These interactions appear either as Friedel cutting or Orowan bypassing wherein their manifestation is governed by particle size. In the case of smaller particle radii, mobile dislocations tend to shear through precipitates. However, as the size of the second phase particle increases, shearing becomes more difficult and mobile dislocations bow around precipitates through Orowan looping [56,57]. In this scenario, elastic interactions between a dislocation and non-deforming precipitates effectively reduce the particle spacing through loop formation wherein a higher bypassing stress is required to allow the passage of further dislocations [58]. A schematic illustrating this effect can be seen in Fig. 7a, where Fig. 7a(i) shows the contact between mobile dislocations and a non-deforming precipitate. The bowing effect with continual dislocation motion under stress is shown in Fig. 7a(ii), and the eventual dislocation bypassing (Fig. 7a(iii)) where the dislocation loop is formed (Fig. 7a(iv)). This effect can be modeled using the following relationship:

$$\tau = \frac{Gb}{L - 2r} \tag{1}$$

where τ is the shear yield strength, G is the material's shear stress, L is the distance between pinning points, and r is the precipitate radius. Examples of dislocation loops discovered in the material subject to cyclic thermal and strain input (AM-4LP-3HT-E) are depicted in Fig. 7. Fig. 7b shows isolated looping events located in the top ~600 nm of the material. Sub-surface instances of looping were also identified, depicted in Fig. 7c. It appears tightly packed precipitates presented as an effective barrier to dislocation motion with instances of looping occurring in close proximity to each other. The formation of dislocation loops has also resulted in the formation of dislocation tangles following bowing. Fig. 7d illustrates this event where a comparably large dislocation forest is located behind the loop. According to Ashby, and Brown and Stobbs, these dislocations produce work-hardening effects as a result of the generation of compressive stress fields at these locations [59,60].

In cases where mobile dislocations interact with precipitates below the critical precipitate size at which bowing occurs, a shearing mechanism takes place wherein a dislocation passes through the precipitate. This phenomenon, known as Friedel cutting can be modeled using the following relationship for the threshold shear stress needed to deform a particle [61]:

$$\tau = cG\varepsilon^{\frac{3}{2}}\left(\frac{rf}{b}\right)^{\frac{1}{2}} \tag{2}$$

where τ is the threshold shear stress, c is the solute atom concentration, G is the material's shear modulus, ε is the misfit strain, r is the precipitate radius, f is the precipitate volume fraction, and b is the Burger's vector. Fig. 8a illustrates this phenomenon as dislocation motion driven by sufficient stress effectively shears a precipitate. An example a precipitated particle being sheared in the AM-4LP-3HT-E sample can be seen in Fig. 8b. In this scenario, where a dislocation encounters a deformable precipitate and successfully passes through it, a new particle-matrix interface is produced accompanied by a change in surface energy producing work hardening effects [61].

5. Conclusion

Additively manufactured Inconel 718 treated with a novel, modified laser peening technique comprising cyclic laser peening and intervening heat treatments was analyzed in order to observe process-induced microstructural modifications owing to the observed thermal stability and property enhancement. TEM investigations uncovered dislocation-particle interactions resulting in pinning, bypassing, and shearing which would not be present without the inclusion of intermittent thermal exposure. In AM-4LP-3HT-E, cyclic strain input was found to effectively lower the solvus temperature of critical intermediate phases including γ'' and δ, leading to increased γ'' content and the availability of δ-phases through γ''→δ transformation. In addition, δ-pinning effects as well as Orowan and Friedel strengthening mechanisms were visualized throughout the treated material. The results presented herein

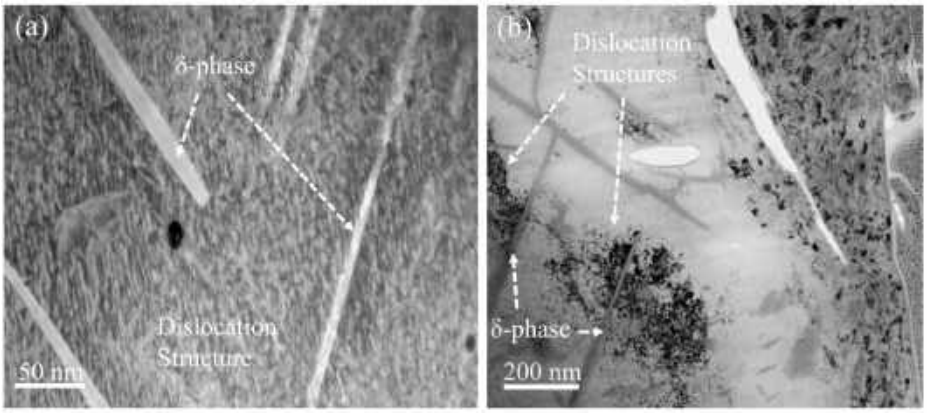

Fig. 6. Examples of δ-phase precipitation pinning identified in (a) AM-LP and (b) AM-4LP-3HT-E.

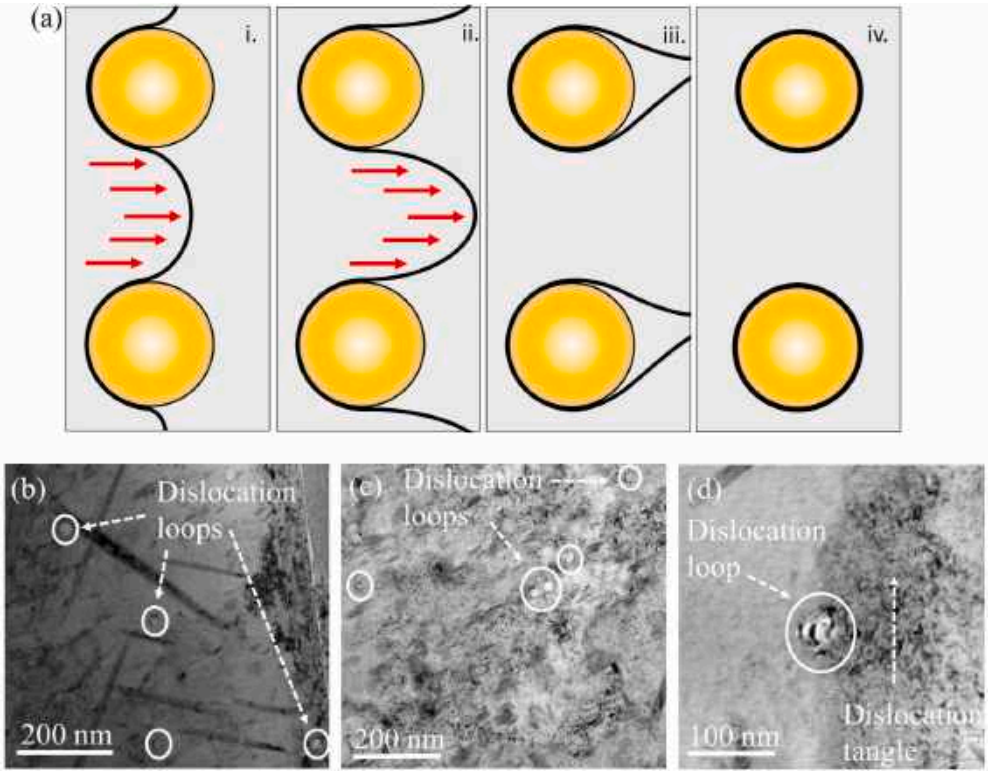

Fig. 7. (a) Schematic of dislocation movement during the Orowan bypassing mechanism; dislocation loops identified in AM-4LP-3HT-E at (b) the treated surface, (c) immediate sub-surface, and (d) an example of dislocation tangle forming behind a dislocation loop.

indicate that these mechanisms enabled the retention of compressive residual stress enhancements from 167.13 MPa to over 300 MPa in material subject to LP + TME. Surface and sub-surface microhardness was also observed to increase from 490 HV (as-built) to 600 HV after cyclic treatment, a nearly 25% increase. It is believed the findings of this work may aid in the development of modified LP processes tailored to delivering thermally-stable material modifications.

Data availability statement

The raw/processed data required to reproduce these findings can be obtained upon request to the corresponding author.

CRediT authorship contribution statement

Michael Munther: Writing - original draft, wrote the manuscript with contributions of Russell Rowe, conducted microstructure characterization. **Russell A. Rowe:** conducted microstructure characterization. **Montu Sharma:** conducted the residual stress measurement. **Lloyd Hackel:** developed the technique. **Keivan Davami:** Writing - original draft, designed the experiments to understand the mechanism behind the technique, wrote the manuscript with contributions of Russell Rowe, The project was directed by Keivan Davami.

Declaration of competing interest

The authors declare that they have no known competing financial interests or personal relationships that could have appeared to influence the work reported in this paper.

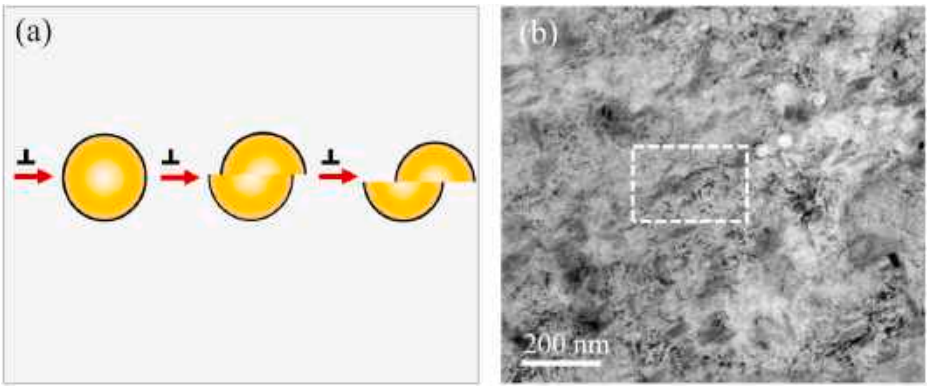

Fig. 8. (a) Schematic illustrating precipitate shearing, and (b) identified example of γ'' shearing in the AM-4LP-3HT-E sample.

Acknowledgements

The authors would like to recognize the Alabama Transportation Institute for providing support for the individuals involved in this work.

References

[1] J.T. Wang, et al., Improving creep properties of 7075 aluminum alloy by laser shock peening, Surf. Coating. Technol. 349 (2018) 725–735.
[2] O. Hatamleh, J. Lyons, R. Forman, Laser and shot peening effects on fatigue crack growth in friction stir welded 7075-T7351 aluminum alloy joints, Int. J. Fatig. 29 (2007) 421–434.
[3] S. Zabeen, M. Preuss, P.J. Withers, Evolution of a laser shock peened residual stress field locally with foreign object damage and subsequent fatigue crack growth, Acta Mater. 83 (2015) 216–226.
[4] B. Lin, C. Lupton, S. Spanrad, J. Schofield, J. Tong, Fatigue crack growth in laser-shock-peened Ti-6Al-4V aerofoil specimens due to foreign object damage, Int. J. Fatig. 59 (2014) 23–33.
[5] J.Z. Lu, et al., Effects of laser peening on stress corrosion cracking (SCC) of ANSI 304 austenitic stainless steel, Corrosion Sci. 60 (2012) 145–152.
[6] O. Hatamleh, P.M. Singh, H. Garmestani, Stress corrosion cracking behavior of peened friction stir welded 2195 aluminum alloy joints, J. Mater. Eng. Perform. 18 (2009) 406–413.
[7] Z. Zhou, et al., A finite element study of thermal relaxation of residual stress in laser shock peened IN718 superalloy, Int. J. Impact Eng. 38 (2011) 590–596.
[8] B.B. Amrinder Singh Gill, A Study of the Effects of Laser Shock Peening on Residual Stress, Microstructure and Local Properties of IN718 Ni-Base Superalloy, 2012.
[9] W. Cao, M. Khadhraoui, B. Brenier, J.Y. Guédou, L. Castex, Thermomechanical relaxation of residual stress in shot peened nickel base superalloy, Mater. Sci. Technol. (United Kingdom) 10 (1994) 947–954.
[10] V. Schulze, Modern Mechanical Surface Treatment, Wiley, 2005, https://doi.org/10.1002/3527607811.
[11] B.J. Foss, et al., Analysis of shot-peening and residual stress relaxation in the nickel-based superalloy RR1000, Acta Mater. 61 (2013) 2548–2559.
[12] Z. Zhou, et al., Thermal relaxation of residual stress in laser shock peened Ti-6Al-4V alloy, Surf. Coating. Technol. 206 (2012) 4619–4627.
[13] J.C.M. Li, Dislocation dynamics IN deformation and recovery, Can. J. Phys. 45 (1967) 493–509.
[14] Z.P. Tong, et al., Effect of laser shock peening on wear behaviors of TC11 alloy at elevated temperature, Optic Laser. Technol. 109 (2019) 139–148.
[15] M. Kattoura, S.R. Mannava, D. Qian, V.K. Vasudevan, Effect of laser shock peening on elevated temperature residual stress, microstructure and fatigue behavior of ATI 718Plus alloy, Int. J. Fatig. 104 (2017) 366–378.
[16] A. Telang, A.S. Gill, S.R. Mannava, D. Qian, V.K. Vasudevan, Effect of temperature on microstructure and residual stresses induced by surface treatments in Inconel 718 SPF, Surf. Coating. Technol. 344 (2018) 93–101.
[17] Y. Li, et al., The strengthening mechanism of a nickel-based alloy after laser shock processing at high temperatures, Sci. Technol. Adv. Mater. 14 (2013).
[18] R.K. Nalla, et al., On the influence of mechanical surface treatments-deep rolling and laser shock peening-on the fatigue behavior of Ti-6Al-4V at ambient and elevated temperatures, Mater. Sci. Eng. A 355 (2003) 216–230.
[19] M. Kattoura, S.R. Mannava, D. Qian, V.K. Vasudevan, Effect of laser shock peening on elevated temperature residual stress, microstructure and fatigue behavior of ATI 718Plus alloy, Int. J. Fatig. 104 (2017) 366–378.
[20] M. Kattoura, S.R. Mannava, D. Qian, V.K. Vasudevan, Effect of laser shock peening on residual stress, microstructure and fatigue behavior of ATI 718Plus alloy, Int. J. Fatig. 102 (2017) 121–134.
[21] P.S. Prevéy, The Effect of Cold Work on The Thermal Stability of Residual Compression in Surface Enhanced In718, 2000.
[22] L. Hackel, J.R. Rankin, A. Rubenchik, W.E. King, M. Matthews, Laser peening: a tool for additive manufacturing post-processing, Addit. Manuf. 24 (2018) 67–75.
[23] C. Ye, Y. Liao, G.J. Cheng, Warm laser shock peening driven nanostructures and their effects on fatigue performance in aluminium alloy 6160, Adv. Eng. Mater. 12 (NA-NA) (2010).
[24] C. Ye, Y. Liao, S. Suslov, D. Lin, G.J. Cheng, Ultrahigh dense and gradient nano-precipitates generated by warm laser shock peening for combination of high strength and ductility, Mater. Sci. Eng. A 609 (2014) 195–203.
[25] J.Z. Zhou, et al., Effects of warm laser peening at elevated temperature on the low-cycle fatigue behavior of Ti6Al4V alloy, Mater. Sci. Eng. A 643 (2015) 86–95.
[26] C. Ye, S. Suslov, B.J. Kim, E.A. Stach, G.J. Cheng, Fatigue performance improvement in AISI 4140 steel by dynamic strain aging and dynamic precipitation during warm laser shock peening, Acta Mater. 59 (2011) 1014–1025.
[27] G. Tani, L. Orazi, A. Fortunato, A. Ascari, G. Campana, Warm laser shock peening: new developments and process optimization, CIRP Ann. - Manuf. Technol. 60 (2011) 219–222.
[28] Y. Liao, C. Ye, G.J. Cheng, [INVITED] A review: warm laser shock peening and related laser processing technique, Optic Laser. Technol. 78 (2016) 15–24.
[29] Y. Liao, G.J. Cheng, Controlled precipitation by thermal engineered laser shock peening and its effect on dislocation pinning: multiscale dislocation dynamics simulation and experiments, Acta Mater. 61 (2013) 1957–1967.
[30] Y. Liao, S. Suslov, C. Ye, G.J. Cheng, The mechanisms of thermal engineered laser shock peening for enhanced fatigue performance, Acta Mater. 60 (2012) 4997–5009.
[31] J. Ginsztler, R.P. Skelton, Component Reliability under Creep-Fatigue Conditions. Component Reliability under Creep-Fatigue Conditions, Springer Vienna, 1998, https://doi.org/10.1007/978-3-7091-2516-8.
[32] Y.L. Kuo, S. Horikawa, K. Kakehi, The effect of interdendritic δ phase on the mechanical properties of Alloy 718 built up by additive manufacturing, Mater. Des. 116 (2017) 411–418.
[33] C.-M. Kuo, Y.-T. Yang, H.-Y. Bor, C.-N. Wei, C.-C. Tai, Aging effects on the microstructure and creep behavior of Inconel 718 superalloy, Mater. Sci. Eng. A 510–511 (2009) 289–294.
[34] J.M. Oblak, D.F. Paulonis, D.S. Duvall, Coherency strengthening in Ni base alloys hardened by DO22 γ′ precipitates, Metall. Trans. 5 (1974) 143–153.
[35] Y. Sun, S. Xu, A. Shan, Effects of annealing on microstructure and mechanical properties of nano-grained Ni-based alloy produced by severe cold rolling, Mater. Sci. Eng. A 641 (2015) 181–188.
[36] K. Kulawik, P.A. Buffat, A. Kruk, A.M. Wusatowska-Sarnek, A. Czyrska-Filemonowicz, Imaging and characterization of γ′ and γ″ nanoparticles in Inconel 718 by EDX elemental mapping and FIB-SEM tomography, Mater. Char. 100 (2015) 74–80.
[37] W.C. Liu, et al., Relationship between the lattice constant of ϒ phase and the content of δ phase, γ″ and γ′ phases in Inconel 718, Scripta Mater. 37 (1997) 59–64.
[38] D.W. Brown, et al., Neutron diffraction measurements of residual stress in additively manufactured stainless steel, Mater. Sci. Eng. A 678 (2016) 291–298.
[39] D.A. Lesyk, et al., Post-processing of the Inconel 718 alloy parts fabricated by selective laser melting: effects of mechanical surface treatments on surface topography, porosity, hardness and residual stress, Surf. Coating. Technol. 381 (2020) 125136.
[40] L.M. Sochalski-Kolbus, et al., Comparison of residual stresses in inconel 718 simple parts made by electron beam melting and direct laser metal sintering, Metall. Mater. Trans. A Phys. Metall. Mater. Sci. 46 (2015) 1419–1432.
[41] I. van Zyl, I. Yadroitsava, I. Yadroitsev, Residual stress in TI6AL4V objects produced by direct metal laser sintering, S. Afr. J. Ind. Eng. 27 (2016) 134–141.
[42] A.S. Gill, A. Telang, V.K. Vasudevan, Characteristics of surface layers formed on inconel 718 by laser shock peening with and without a protective coating, J. Mater. Process. Technol. 225 (2015) 463–472.
[43] P. Peyre, R. Fabbro, P. Merrien, H.P. Lieurade, Laser shock processing of aluminium alloys. Application to high cycle fatigue behaviour, Mater. Sci. Eng. A 210 (1996) 102–113.
[44] A. Telang, A.S. Gill, S.R. Mannava, D. Qian, V.K. Vasudevan, Effect of temperature on microstructure and residual stresses induced by surface treatments in Inconel 718 SPF, Surf. Coating. Technol. 344 (2018) 93–101.

[45] S. Azadian, L.Y. Wei, R. Warren, Delta phase precipitation in inconel 718, Mater. Char. 53 (2004) 7–16.
[46] Y. Mei, et al., Effects of cold rolling on the precipitation kinetics and the morphology evolution of intermediate phases in Inconel 718 alloy, J. Alloys Compd. 649 (2015) 949–960.
[47] W. Chen, M.C. Chaturvedi, On the mechanism of serrated deformation in aged Inconel 718, Mater. Sci. Eng. A 229 (1997) 163–168.
[48] C.L. Hale, W.S. Rollings, M.L. Weaver, Activation energy calculations for discontinuos yielding in inconel 718SPF, Mater. Sci. Eng. A 300 (2001) 153–164.
[49] Y.K. Jeong, C.Y. Jo, Y.H. Kim, I.B. Kim, Effects of cold drawing ratio on δ phase precipitation behaviors of alloy 718 wire, Met. Mater. Int. 3 (1997) 224–229.
[50] A.C. Yeh, K.W. Lu, C.M. Kuo, H.Y. Bor, C.N. Wei, Effect of serrated grain boundaries on the creep property of Inconel 718 superalloy, Mater. Sci. Eng. A 530 (2011) 525–529.
[51] Y.C. Lin, J. Deng, Y.Q. Jiang, D.X. Wen, G. Liu, Hot tensile deformation behaviors and fracture characteristics of a typical Ni-based superalloy, Mater. Des. 55 (2014) 949–957.
[52] J. Calvo, M. Penalva, J.M. Cabrera, Characterization of strain-induced precipitation in inconel 718 superalloy, J. Mater. Eng. Perform. 25 (2016) 3409–3417.
[53] M. Anderson, A.L. Thielin, F. Bridier, P. Bocher, J. Savoie, δ Phase precipitation in Inconel 718 and associated mechanical properties, Mater. Sci. Eng. A 679 (2017) 48–55.
[54] Y.C. Lin, J. Deng, Y.Q. Jiang, D.X. Wen, G. Liu, Effects of initial δ phase on hot tensile deformation behaviors and fracture characteristics of a typical Ni-based superalloy, Mater. Sci. Eng. A 598 (2014) 251–262.
[55] N.D. Evans, P.J. Maziasz, R.W. Swindeman, G.D. Smith, Microstructure and phase stability in INCONEL alloy 740 during creep, Scripta Mater. 51 (2004) 503–507.
[56] Z. Zhang, D.L. Chen, Consideration of Orowan strengthening effect in particulate-reinforced metal matrix nanocomposites: a model for predicting their yield strength, Scripta Mater. 54 (2006) 1321–1326.
[57] S. Queyreau, G. Monnet, B. Devincre, Orowan strengthening and forest hardening superposition examined by dislocation dynamics simulations, Acta Mater. 58 (2010) 5586–5595.
[58] R.O. Scattergood, D.J. Bacon, The Orowan mechanism in anisotropic crystals, Philos. Mag. A 31 (1975) 179–198.
[59] L.M. Brown, Precipitation and dispersion hardening, in: *Energy Technology Review* 1551–1571, Pergamon Press (Int Ser on the Strength and Fract of Mater and Struct), 1980, https://doi.org/10.1016/b978-1-4832-8412-5.50245-9.
[60] M.F. Ashby, The deformation of plastically non-homogeneous materials, Philos. Mag. A 21 (1970) 399–424.
[61] J. Friedel, Dislocations, Pergamon Press, 1964.